Published in final edited form as:
J Biomech. 2010 August 26; 43(12): 2254–2260. doi:10.1016/j.jbiomech.2010.02.038.

The Influence of Prior Hamstring Injury on Lengthening Muscle Tissue Mechanics

Amy Silder[1], **Scott B. Reeder**[1,2,3,4], and **Darryl G. Thelen**[1,5,6]

[1]Department of Biomedical Engineering, University of Wisconsin-Madison, Madison, WI

[2]Department of Radiology, University of Wisconsin-Madison, Madison, WI

[3]Department of Medical Physics, University of Wisconsin-Madison, Madison, WI

[4]Department of Medicine, University of Wisconsin-Madison, Madison, WI

[5]Department of Mechanical Engineering, University of Wisconsin-Madison, Madison, WI

[6]Department of Orthopedics and Rehabilitation, University of Wisconsin-Madison, Madison, WI

Abstract

Hamstring strain injuries often occur near the proximal musculotendon junction (MTJ) of the biceps femoris. Post-injury remodeling can involve scar tissue formation, which may alter contraction mechanics and influence re-injury risk. The purpose of this study was to assess the affect of prior hamstring strain injury on muscle tissue displacements and strains during active lengthening contractions. Eleven healthy and eight subjects with prior biceps femoris injuries were tested. All previously injured subjects had since returned to sport and exhibited evidence of residual scarring along the proximal aponeurosis. Subjects performed cyclic knee flexion-extension on an MRI-compatible device using elastic and inertial loads, which induced active shortening and lengthening contractions, respectively. CINE phase-contrast imaging was used to measure tissue velocities within the biceps femoris during these tasks. Numerical integration of the velocity information was used to estimate two-dimensional tissue displacement and strain fields during muscle lengthening. The largest tissue motion was observed along the distal MTJ, with the active lengthening muscle exhibiting significantly greater and more homogeneous tissue displacements. First principal strains magnitudes were largest along the proximal MTJ for both loading conditions. The previously injured subjects exhibited less tissue motion and significantly greater strains near the proximal MTJ. We conclude that localized regions of high tissue strains during active lengthening contractions may predispose the proximal biceps femoris to injury. Furthermore, post-injury remodeling may alter the in-series stiffness seen by muscle tissue and contribute to the relatively larger localized tissue strains near the proximal MTJ, as was observed in this study.

Please address correspondence to: Darryl G. Thelen, Department of Mechanical Engineering, 1513 University Ave., Madison, WI 53706, Phone: (608) 262-1902, Fax: (608) 265-2316, thelen@engr.wisc.edu.

CONFILCT OF INTEREST

None of the authors have any financial or personal relationships with other people or organizations that could inappropriately influence the quality of the work presented in this manuscript.

Keywords

phase contrast velocity; magnetic resonance imaging; hamstring muscle; muscle strain

INTRODUCTION

Acute muscle strain injuries are frequent in sporting activities, with hamstring injuries particularly common among athletes who sprint regularly. It is well established that muscle is most susceptible to injury during active lengthening contractions (Lieber et al., 1991; Friden and Lieber, 2001; Kirkendall and Garrett, 2002). Correspondingly, hamstring injuries are thought to occur during the late swing phase of sprinting (Heiderscheit et al., 2005; Thelen et al., 2005), when the hamstrings are active, lengthening, and subjected to large inertial loads (Simonsen et al., 1985; Mann et al., 1986).

Hamstring injuries most commonly involve the proximal musculotendon junction (MTJ) of the biceps femoris long head (BFLH) (Schneider-Kolsky et al., 2006; Verrall et al., 2006; Koulouris et al., 2007; Silder et al., 2008). In-situ animal studies have shown that acute strain injuries do not involve an actual separation between muscle and tendon, but rather the muscle tissue adjacent to the MTJ is damaged (Garrett et al., 1987). Following injury, the highly vascularized muscle tissue quickly begins regenerating (Kaariainen et al., 2000). However, within a week's time, the growth of fibrous tissue begins to prevail over the muscle regeneration process and eventually leads to the presence of mature acellular scar at the site of injury (Nikolaou et al., 1987; Jarvinen et al., 2005). This scar tissue can persist indefinitely, having been found up to 12 months post-injury in animal models (Kaariainen et al., 2000). Similarly, in humans, magnetic resonance (MR) imaging has shown evidence of scar tissue up to one year following an athlete's return to sport (Silder et al., 2008). The presence of scar tissue can alter muscle force transmission paths (Huijing, 2003), and may decrease the compliance of the tendon/aponeurosis complex. This, in turn, could change the deformation patterns within muscle tissue. Given the links between tissue strain magnitudes and injury risk observed in animal models (Lieber and Friden, 1993), one concern would be an increase in localized tissue strains adjacent to the fibrous scar. Such an effect, if present, may contribute to the high re-injury rates (~30%) that are observed when athletes return to sport following an acute hamstring injury (Orchard and Best, 2002; Woods et al., 2004).

The purpose of this study was to assess the influence of prior hamstring injury on *in-vivo* muscle deformation patterns during active lengthening contractions. Dynamic MR imaging techniques (Pappas et al., 2002; Asakawa et al., 2003; Finni et al., 2003) were used to track biceps femoris muscle tissue displacements during a knee flexion-extension task that included active lengthening hamstring contractions. Tissue displacement data were spatially differentiated to estimate two-dimensional strain distributions (Zhou and Novotny, 2007; Zhong et al., 2008). Muscle tissue strains were then used to address two specific research aims. First, we tested the hypothesis that the largest tissue strains would be observed along the proximal MTJ, where muscle injury is commonly observed. Second, we examined the effects of residual scar tissue on neighboring muscle tissue strain by comparing a group of uninjured athletes to those with prior hamstring injuries.

METHODS

Subjects

The right limbs of 11 healthy subjects (5 males, 6 females; age 31±11y; height 1.77±0.09m; mass 70±9kg) and the previously injured limbs (left or right) of eight subjects (6 males, 2 females, age 23±6; height 1.80±0.10m; mass 75±11kg) were evaluated. Subject questioning

and clinical reports confirmed that all previously injured subjects sustained at least one proximal biceps femoris injury, with six of the eight reporting one or more re-injuries in the same location. Three subjects had histories of bilateral hamstring injuries. For these subjects, dynamic imaging was performed on the limb that was more severely injured, as assessed by total time from sport (Slavotinek et al., 2002). Informed consent was obtained prior to testing according to a protocol approved by the University of Wisconsin's Health Sciences Institutional Review Board.

We required that all previously injured subjects present with visible remodeling of the proximal biceps femoris tendon/aponeurosis (Fig. 1). The presence of post-injury remodeling was assessed by collecting high resolution static images of both limbs using an investigational version of a previously described T_1 weighted chemical shift based water-fat separation method known as IDEAL (Iterative Decomposition of water and fat with Echo Asymmetry and Least squares estimation) combined with three-dimensional (3D) spoiled gradient echo (SPGR) imaging (Reeder et al., 2007). IDEAL provides water-only images with uniform suppression of fat-signal over large fields-of-view. All subjects were scanned in a relaxed prone position using a clinical 1.5T MR scanner (Signa HDx v14.0 TwinSpeed, GE Healthcare, Waukesha, WI). A phased array torso coil was used with the following scan parameters: coronal 3D slab, TR=12.5ms, 3 echoes (1 echo/TR) with TE=4.4, 5.0, 6.6ms, 15° flip angle; matrix, ±41.7kHz bandwidth, partial k_y acquisition; 384×256 matrix with 46×46cm field-of-view with 84 slices, and 1.4mm slice thickness for a true spatial resolution of $1.2\times1.8\times1.4mm^3$ (interpolated to $0.9\times0.9\times7mm^3$). Water and fat images were created using homodyne reconstruction performed on-line (Reeder et al., 2005;Yu et al., 2005). The IDEAL image set was used to perform a bilateral comparison of the proximal biceps femoris tendon/aponeurosis. Injury location and residual effects were confirmed if substantial non-uniformity in tendon/aponeurosis size was present between limbs.

Dynamic Imaging Protocol

Dynamic images were obtained with the subject lying prone on an MR-compatible device (Fig. 2) (Silder et al., 2009). Foam padding was used to position the hip into ~15° of flexion. The knee was aligned with a fixed rotation shaft on the device, and the ankle was secured to two leg braces that extended from that shaft. The device was used to guide the limb through ~30° of sagittal knee motion within the scanner, while imposing either inertial (Fig. 2a) or elastic (Fig. 2b) loads on the hamstrings. In a prior study, we showed that the inertial load induces hamstring muscle activity when the knee is extending, thereby resulting in an active lengthening contraction. In contrast, the elastic load induces hamstring activity when the knee is flexing, such that the hamstrings are relaxing and lengthening while the knee is extending (Silder et al., 2009). To reduce fatigue effects, elastic and inertial load magnitudes were kept relatively low, with knee flexion moments varying cyclically between 0 and ~12 Nm. Peak moments occurred near maximum knee extension in the inertial case and near maximum knee flexion in the elastic case (Silder et al., 2009).

CINE phase-contrast (CINE-PC) imaging was used to measure three-dimensional tissue velocities within an imaging plane that bisected the long axis of the biceps femoris. An oblique-sagittal imaging plane was used for six healthy subjects (Fig. 3a) and an oblique-coronal imaging plane (Fig. 3b) was used for the remaining five healthy and eight previously injured subjects. Compared to the sagittal-oblique imaging plane, the coronal-oblique plane included less of the biceps femoris short head, but a greater cross-sectional area of the proximal BFLH tendon/aponeurosis. All images were collected using a single channel flex wrap coil secured around the posterior thigh. Three trials were conducted for each loading condition at a rate of 28 cycles/min, with each scan lasting 1min 39s. The imaging sequence was gated to the onset of knee flexion using a plethysmograph placed under the ankle. Each scan resulted in one magnitude image and three velocity images per time frame. Scanning

parameters were: TR/TE=5.6/2.4ms, ±62.5kHz bandwidth, 20° flip angle, 256×192 matrix with 40×18cm field-of-view for true spatial resolution 1.6×2.1×6mm, VENC=5cm/s, segmentation factor of 4 lines of k-space per cycle, and 40 reconstructed time frames per cycle.

Dynamic Image Analysis

Reconstruction of all images was performed online, and subsequent displacement and strain calculations were performed offline using MATLAB (The Mathworks Inc., Natick, MA, USA). Dynamic images were analyzed using a mesh based tracking approach (Zhu and Pelc, 1999). For each trial, we first manually identified a region of interest over the visible portion of the BFLH using the frame corresponding to maximum knee flexion. Delauney triangulation was then used to generate a triangular element mesh over the muscle tissue, with edge lengths of ~5mm (Fig. 3c). The node positions in this initial mesh were considered the reference configuration for all subsequent analyses.

At each frame (starting with the reference frame), we identified all image pixels that were within the mesh, and then determined each pixel's coordinates relative to the element of which it belonged. Assuming linear variation of velocity across an element, we then expressed each pixel's velocity as a linear function of the velocities of the three nodes that surrounded the pixel (Zhu and Pelc, 1999). Because the number of pixels (1.6×2.1mm spacing) within the mesh exceeded the number of nodes (~5mm spacing), this process resulted in an over-determined set of linear equations that related nodal velocities to measured pixel velocities. A linear least-squares solution to these equations produced nodal velocities, which were then integrated to find the new nodal positions at the next frame. This process was repeated for all subsequent time frames resulting in two-dimensional nodal trajectories over the entire flexion-extension cycle. This same integration process was also performed using backward time steps. A weighted average of the forward and backward nodal trajectories were input into a closed-loop Fourier integration routine, which enforced cyclic continuity and further refined the trajectory estimates to include higher frequency components (Zhu et al., 1996).

The nodal trajectories, along with the linear element shape functions, were used to compute the two-dimensional deformation gradient tensor $\mathbf{F}$, relative to the initial reference mesh configuration (Zhu and Pelc, 1999). The Lagrangian finite strain tensor, $\mathbf{E}=\frac{1}{2}(\mathbf{F}^{T}\mathbf{F}-\mathbf{I})$, was then calculated for each element in the mesh. The nodal strain tensors were taken as the average of the strains of all elements adjacent to a node. The most positive eignevalue and corresponding eigenvector of the nodal strain tensors were defined as the first principal strain (E_1) and direction ($\mathbf{e_1}$) for that node.

Four spatial regions were established to quantify the distribution of muscle displacements and strains relative to the proximal MTJ. To do this, we manually drew a line along the length of the visible tendon/aponeurosis in the magnitude image of maximum knee flexion (i.e. the reference configuration). Four regions were then defined as the BFLH tissue within 0–1cm, 1–2cm, 2–3cm, and 3–4cm from the proximal tendon/aponeurosis (Fig. 3d). We averaged the following outcome measures within each region: maximum superior-inferior (S-I) tissue displacement, maximum first principal strain magnitudes, and first principal strain directions.

A two-factor repeated measures ANOVAs was used to assess any differences between imaging planes. Displacements and strain magnitudes were found to be not significantly different between the two imaging planes. Therefore, a comparison between subject groups was conducted using a four-factor ANOVA, with repeated measures obtained from the two loading conditions, four muscle regions, and three trials. Similarly, a three-factor ANOVA

with two repeated measures (loading condition, trials) was used to compare these same measures between subject groups across the entire muscle tissue.

RESULTS

Tissue Motion

For both loading conditions, the least amount of S-I tissue displacement was measured along the proximal MTJ ($p<0.01$) (Fig. 4, 6). Furthermore, a load-by-region interaction was observed ($p<0.01$), mainly due to the relatively greater motion along the proximal MTJ for the inertial loading, when compared to the elastic loading condition ($p<0.01$) (Fig. 4). This difference reflected the inertial load inducing greater ($p=0.01$) and more homogenous S-I displacements across the muscle tissue.

Tissue Strains

Maximum first principal tissue strains across the entire BFLH were on the order of ~11%. Muscle tissue adjacent to the proximal MTJ exhibited larger first principal strains ($p<0.01$) than the more distal and lateral tissue (Fig. 5). This result was observed for both inertial and elastic loading conditions. However, compared to the inertial loading condition, computed strains were greater ($p<0.01$) for the elastic loading, reflecting greater muscle tissue elongation during the lengthening phase (Fig. 5).

Injury Effects

Tissue displacement maps were visually distinct between groups, with the injured subjects tending to exhibit a relative decrease in motion along the MTJ (Fig. 6). Compared to the healthy subjects, first principal strains were significantly greater for the injured subjects across the entire muscle tissue ($p<0.01$), as well as within the first three regions nearest the MTJ ($p<0.01$) (Fig. 7).

DISCUSSION

The purpose of this study was to investigate strain distributions within the lengthening BFLH and to assess the influence of prior hamstring strain injury on *in-vivo* muscle tissue mechanics. For all subjects, the largest tissues strains were observed near the proximal MTJ, where acute injury often occurs (Schneider-Kolsky et al., 2006; Verrall et al., 2006; Koulouris et al., 2007; Silder et al., 2008). Moreover, subjects with a prior injury exhibited even larger first principal tissue strains in this region. Given the links between strain magnitude and injury risk (Lieber and Friden, 1993), these results suggest a mechanism by which post-injury muscle remodeling may contribute to the high re-injury risk that is observed when athletes return to sport (Orchard and Best, 2002; Woods et al., 2004).

In un-injured muscle, as fibers approach the MTJ, extensive folding of the sarcolemma increases the surface area available for force transmission to the tendon (Kaariainen et al., 2000), helping to make the MTJ very compliant in tension (Purslow, 2002). However, the sarcolemma is usually damaged during injury, which results in fibrous scar formation, and an increase in relative stiffness of the MTJ (Best and Hunter, 2000; Purslow, 2002). It is believed that the strain in active lengthening muscle tissue depends substantially on tendon compliance (Lieber et al., 1991; Thelen et al., 2005; Fukashiro et al., 2006). Hence, a decrease in the compliance of the tendon-aponeurosis complex could lead to increased strain in nearby muscle tissue, potentially increasing the risk for subsequent injury. In the current study, we measured significantly greater strains in subjects who exhibited an enlarged proximal tendon/aponeurosis (Fig. 1). Assuming the additional tendinous/scar tissue is less compliant that the muscle tissue it replaces, then the post-injury remodeling along the MTJ

may have necessitated the greater stretch in fibers near the prior injury, as observed. We cannot preclude the possibility that the observed group differences in proximal muscle tissue strains simply reflect less compliant tendons that existed prior to injury, rather than a remodeling effect. However, there is some evidence of athletes who regularly use elastic-recoil training having less compliant tendons (Arampatzis et al., 2007), such that this issue deserves further study.

The estimated displacement and strain fields showed substantial heterogeneity throughout the length and width of the muscle, which is consistent with observations made in prior dynamic imaging studies (Asakawa et al., 2002; Pappas et al., 2002; Zhou and Novotny, 2007; Zhong et al., 2008). In particular, the smallest motion was observed along the proximal MTJ and the largest motion was observed along the distal and lateral boundaries of the muscle. Furthermore, load-dependent variations in tissue motion were evident, with greater overall muscle tissue displacements when the muscle was active and lengthening (inertial load), compared to when it was relaxing and lengthening (elastic load) (Fig. 4). This difference is likely attributable to the tendon being loaded, and hence stretching, during active lengthening, which allows the muscle fibers to remain more isometric (Fukunaga et al., 2001; Reeves and Narici, 2003). These observations are consistent with the idea that muscle fibers remain more isometric in active stretch-shortening contractions (Fukunaga et al., 2001; Reeves and Narici, 2003). In contrast, during the elastic loading, the externally applied load decreases during knee extension. This results in tendon unloading, and hence shortening, as the knee extends. As a result, the muscle tissue elongates a relatively greater amount.

It is believed that muscle tissue undergoes substantial shearing between fibers, particularly near a MTJ (Huijing 1999, Blemker 2005). Such shear stresses would facilitate lateral force transmission paths, which may be altered by injury-induced changes in musculotendon morphology and material properties (Huijing, 2003). Such an effect would be reflected in the principal tissue strain directions (Zhong et al., 2008). In this study, we did not observe differences in first or second principal strain directions between the uninjured and previously injured subjects. However, we were only able to quantify principal strains with respect to the long axis of the muscle, rather than the underlying fiber direction, which may be more relevant (Zhong et al. 2008). Observationally, the fascicle direction within the main muscle body could be seen in the IDEAL water images, and seemed to generally align with the principal strain directions (Fig. 8). This implies that positive first principal strains in the muscle belly may primarily represent along fascicle stretch. More quantitative comparisons of principal strain and fiber directions are needed to investigate this issue further, and could potentially be achieved using diffusion tensor imaging techniques (Blemker et al., 2007).

One limitation of dynamic MR imaging is that collagenous tissue, such as tendon and scar, is void of signal and appears as regions of noise in CINE-PC velocity data. As a result, it is not possible to measure tendinous tissue velocity using CINE-PC, and the tracking of muscle tissue motion immediately adjacent to the MTJ is challenging. To address this problem, we initially defined the mesh to be at least one pixel from any low signal tissue surrounding the BFLH and then visually inspected tracked mesh motion thereafter to ensure that it did not enter into the noise regions.

The reliability of displacement data depends on the subject's ability to perform repeatable flexion-extension motion with minimal fatigue. Prior to imaging experiments, we established that both the induced loads and muscle activities were highly repeatable, with less than one degree variation in knee motion over 50+ cycles (Silder et al., 2009). Fatigue effects were addressed by using relatively low loads, which required less than 20% of the subject's isokinetic (30deg/s) knee flexion strength. Statistical comparisons of repeat image

collections revealed no significant differences between trials, suggesting that repeatability was acceptable. There was substantial variability in the magnitude of displacements and strains between subjects (Fig. 5, 7), which is in part due to differences in the knee range of motion that was achievable within the scanner bore. Individual variations in musculotendon architecture and muscle moment arms could also affect the heterogeneous behavior of muscle tissue motion (Blemker and Delp, 2005), and should be explored further.

Our analysis inherently assumed that the predominate muscle tissue motion occurred within a two-dimensional imaging plane. The average absolute value of out-of-plane velocities was 24% of the average S-I velocity, which is similar to the values reported in previous studies (Sheehan et al., 1998; Pappas et al., 2002; Zhou and Novotny, 2007). The development of methods to acquire three-dimensional volumetric data in an acceptable scan time would circumvent this problem, and provide means of evaluating 3D strains through the muscle volume (Wentland, Korosec, Grist, 2006). Furthermore, we were not able to compute absolute tissue strains relative to the muscle's relaxed state. Alternatively, we computed tissue strains relative to the muscle configuration at maximum knee flexion, which differs between the elastic and inertial loading conditions. Recently, several investigators have developed three-dimensional models of musculotendon architecture that can provide estimates of absolute three-dimensional tissue strains (Blemker and Delp, 2005; Fernandez et al., 2005; Yucesoy and Huijing, 2007).

Simulations of muscle contraction during running have shown that the hamstrings undergo an active lengthening contraction when decelerating the limb during the latter half of swing (Thelen et al., 2005), which is likely when the hamstrings are most susceptible to injury (Heiderscheit et al., 2005). The current study showed that increased mechanical strains arise near the proximal biceps femoris MTJ during relatively low-load lengthening contractions, and that subjects with prior injury presented with significantly greater muscle tissue strains, when compared to their healthy counterparts. Taken together, our results suggest that residual scar tissue at the site of a prior musculotendon injury may adversely affect local tissue mechanics in a way that could contribute to risk for re-injury during movement tasks (e.g. running) that involve active lengthening contractions.

Acknowledgments

NIH AR056201, NFL Charities, Christopher Westphal, Kelli Hellenbrand, and Silvia Blemker, PhD.

REFERENCES

Arampatzis A, Karamanidis K, Morey-Klapsing G, De Monte G, Stafilidis S. Mechanical properties of the triceps surae tendon and aponeurosis in relation to intensity of sport activity. J Biomech. 2007; 40(9):1946–1952. [PubMed: 17101142]

Asakawa DS, Blemker SS, Gold GE, Delp SL. In vivo motion of the rectus femoris muscle after tendon transfer surgery. J Biomech. 2002; 35(8):1029–1037. [PubMed: 12126662]

Asakawa DS, Pappas GP, Blemker SS, Drace JE, Delp SL. Cine phase-contrast magnetic resonance imaging as a tool for quantification of skeletal muscle motion. Seminars in Musculoskeletal Radiology. 2003; 7(4):287–295. [PubMed: 14735427]

Best TM, Hunter KD. Muscle injury and repair. Phys Med Rehabil Clin N Am. 2000; 11(2):251–266. [PubMed: 10810760]

Blemker SS, Asakawa DS, Gold GE, Delp SL. Image-based musculoskeletal modeling: applications, advances, and future opportunities. J Magn Reson Imaging. 2007; 25(2):441–451. [PubMed: 17260405]

Blemker SS, Delp SL. Three-dimensional representation of complex muscle architectures and geometries. Ann Biomed Eng. 2005; 33(5):661–673. [PubMed: 15981866]

Fernandez JW, Buist ML, Nickerson DP, Hunter PJ. Modelling the passive and nerve activated response of the rectus femoris muscle to a flexion loading: a finite element framework. Med Eng Phys. 2005; 27(10):862–870. [PubMed: 15869895]

Finni T, Hodgson JA, Lai AM, Edgerton VR, Sinha S. Nonuniform strain of human soleus aponeurosis-tendon complex during submaximal voluntary contractions in vivo. J Appl Physiol. 2003; 95(2):829–837. [PubMed: 12716873]

Friden J, Lieber RL. Eccentric exercise-induced injuries to contractile and cytoskeletal muscle fibre components. Acta Physiol Scand. 2001; 171(3):321–326. [PubMed: 11412144]

Fukashiro S, Hay DC, Nagano A. Biomechanical behavior of muscle-tendon complex during dynamic human movements. J Appl Biomech. 2006; 22(2):131–147. [PubMed: 16871004]

Fukunaga T, Kubo K, Kawakami Y, Fukashiro S, Kanehisa H, Maganaris CN. In vivo behaviour of human muscle tendon during walking. Proc R Soc Lond B Biol Sci. 2001; 268(1464):229–233.

Garrett WE Jr, Safran MR, Seaber AV, Glisson RR, Ribbeck BM. Biomechanical comparison of stimulated and nonstimulated skeletal muscle pulled to failure. Am J Sports Med. 1987; 15(5): 448–454. [PubMed: 3674268]

Heiderscheit BC, Hoerth DM, Chumanov ES, Swanson SC, Thelen BJ, Thelen DG. Identifying the time of occurrence of a hamstring strain injury during treadmill running: a case study. Clin Biomech (Bristol, Avon). 2005; 20(10):1072–1078.

Huijing PA. Muscular force transmission necessitates a multilevel integrative approach to the analysis of function of skeletal muscle. Exerc Sport Sci Rev. 2003; 31(4):167–175. [PubMed: 14571955]

Jarvinen TA, Jarvinen TL, Kaariainen M, Kalimo H, Jarvinen M. Muscle injuries: biology and treatment. Am J Sports Med. 2005; 33(5):745–764. [PubMed: 15851777]

Kaariainen M, Jarvinen T, Jarvinen M, Rantanen J, Kalimo H. Relation between myofibers and connective tissue during muscle injury repair. Scand J Med Sci Sports. 2000; 10(6):332–337. [PubMed: 11085560]

Kirkendall DT, Garrett WE Jr. Clinical perspectives regarding eccentric muscle injury. Clin Orthop. 2002; (403 Suppl):S81–S89. [PubMed: 12394456]

Koulouris G, Connell DA, Brukner P, Schneider-Kolsky M. Magnetic resonance imaging parameters for assessing risk of recurrent hamstring injuries in elite athletes. Am J Sports Med. 2007; 35(9): 1500–1506. [PubMed: 17426283]

Lieber RL, Friden J. Muscle damage is not a function of muscle force but active muscle strain. Journal of Applied Physiology. 1993; 74(2):520–526. [PubMed: 8458765]

Lieber RL, Leonard ME, Brown CG, Trestik CL. Frog semitendinosis tendon load-strain and stress-strain properties during passive loading. Am J Physiol. 1991; 261(1 Pt 1):C86–C92. [PubMed: 1858862]

Lieber RL, Woodburn TM, Friden J. Muscle damage induced by eccentric contractions of 25% strain. J Appl Physiol. 1991; 70(6):2498–2507. [PubMed: 1885443]

Mann RA, Moran GT, Dougherty SE. Comparative electromyography of the lower extremity in jogging, running, and sprinting. Am J Sports Med. 1986; 14(6):501–510. [PubMed: 3799879]

Nikolaou PK, Macdonald BL, Glisson RR, Seaber AV, Garrett WE Jr. Biomechanical and histological evaluation of muscle after controlled strain injury. Am J Sports Med. 1987; 15(1):9–14. [PubMed: 3812867]

Orchard J, Best TM. The management of muscle strain injuries: an early return versus the risk of recurrence. Clinical Journal of Sport Medicine. 2002; 12(1):3–5. [PubMed: 11854581]

Pappas GP, Asakawa DS, Delp SL, Zajac FE, Drace JE. Nonuniform shortening in the biceps brachii during elbow flexion. J Appl Physiol. 2002; 92(6):2381–2389. [PubMed: 12015351]

Purslow PP. The structure and functional significance of variations in the connective tissue within muscle. Comp Biochem Physiol A Mol Integr Physiol. 2002; 133(4):947–966. [PubMed: 12485685]

Reeder SB, Hargreaves BA, Yu H, Brittain JH. Homodyne reconstruction and IDEAL water-fat decomposition. Magn Reson Med. 2005; 54(3):586–593. [PubMed: 16086311]

Reeder SB, McKenzie CA, Pineda AR, Yu H, Shimakawa A, Brau AC, Hargreaves BA, Gold GE, Brittain JH. Water-fat separation with IDEAL gradient-echo imaging. J Magn Reson Imaging. 2007; 25(3):644–652. [PubMed: 17326087]

Reeves ND, Narici MV. Behavior of human muscle fascicles during shortening and lengthening contractions in vivo. J Appl Physiol. 2003; 95(3):1090–1096. [PubMed: 12740314]

Schneider-Kolsky ME, Hoving JL, Warren P, Connell DA. A comparison between clinical assessment and magnetic resonance imaging of acute hamstring injuries. Am J Sports Med. 2006; 34(6):1008–1015. [PubMed: 16476919]

Sheehan FT, Zajac FE, Drace JE. Using cine phase contrast magnetic resonance imaging to non-invasively study in vivo knee dynamics. J Biomech. 1998; 31(1):21–26. [PubMed: 9596534]

Silder A, Heiderscheit BC, Thelen DG, Enright T, Tuite MJ. MR observations of long-term musculotendon remodeling following a hamstring strain injury. Skeletal Radiol. 2008; 37(12): 1101–1109. [PubMed: 18649077]

Silder A, Westphal C, Thelen D. A MR-Compatible Loading Device for Dynamically Imaging Shortening and Lengthening Muscle Contraction Mechanics. J Med Devices. 2009; 3(3)

Simonsen EB, Thomsen L, Klausen K. Activity of mono- and biarticular leg muscles during sprint running. Eur J Appl Physiol Occup Physiol. 1985; 54(5):524–532. [PubMed: 4085483]

Slavotinek JP, Verrall GM, Fon GT. Hamstring injury in athletes: using MR imaging measurements to compare extent of muscle injury with amount of time lost from competition. AJR. American Journal of Roentgenology. 2002; 179(6):1621–1628. [PubMed: 12438066]

Thelen DG, Chumanov ES, Best TM, Swanson SC, Heiderscheit BC. Simulation of biceps femoris musculotendon mechanics during the swing phase of sprinting. Med Sci Sports Exerc. 2005; 37(11):1931–1938. [PubMed: 16286864]

Thelen DG, Chumanov ES, Hoerth DM, Best TM, Swanson SC, Li L, Young M, Heiderscheit BC. Hamstring muscle kinematics during treadmill sprinting. Med Sci Sports Exerc. 2005; 37(1):108–114. [PubMed: 15632676]

Verrall GM, Slavotinek JP, Barnes PG, Fon GT, Esterman A. Assessment of physical examination and magnetic resonance imaging findings of hamstring injury as predictors for recurrent injury. J Orthop Sports Phys Ther. 2006; 36(4):215–224. [PubMed: 16676871]

Woods C, Hawkins RD, Maltby S, Hulse M, Thomas A, Hodson A. The Football Association Medical Research Programme: an audit of injuries in professional football--analysis of hamstring injuries. Br J Sports Med. 2004; 38(1):36–41. [PubMed: 14751943]

Yu H, Reeder SB, Shimakawa A, Brittain JH, Pelc NJ. Field map estimation with a region growing scheme for iterative 3-point water-fat decomposition. Magn Reson Med. 2005; 54(4):1032–1039. [PubMed: 16142718]

Yucesoy CA, Huijing PA. Substantial effects of epimuscular myofascial force transmission on muscular mechanics have major implications on spastic muscle and remedial surgery. J Electromyogr Kinesiol. 2007; 17(6):664–679. [PubMed: 17395489]

Zhong X, Epstein FH, Spottiswoode BS, Helm PA, Blemker SS. Imaging two-dimensional displacements and strains in skeletal muscle during joint motion by cine DENSE MR. J Biomech. 2008; 41(3):532–540. [PubMed: 18177655]

Zhou H, Novotny JE. Cine phase contrast MRI to measure continuum Lagrangian finite strain fields in contracting skeletal muscle. J Magn Reson Imaging. 2007; 25(1):175–184. [PubMed: 17152055]

Zhu Y, Drangova M, Pelc NJ. Fourier tracking of myocardial motion using cine-PC data. Magn Reson Med. 1996; 35(4):471–480. [PubMed: 8992196]

Zhu Y, Pelc NJ. A spatiotemporal model of cyclic kinematics and its application to analyzing nonrigid motion with MR velocity images. IEEE Trans Med Imaging. 1999; 18(7):557–569. [PubMed: 10504090]

Figure 1.
High resolution static images were obtained for all subjects and used to assess bilateral asymmetries in hamstring morphology. This example shows the visible differences in tendon/aponeurosis morphology at the site of prior injury that was evident for all of the previously injured subjects.

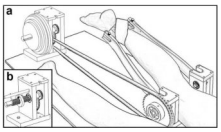

Figure 2.

A MR-compatible device was used during dynamic MR-imaging. Subjects lay prone on the device, with their knee joint aligned with a fixed rotation shaft on the device. The ankle was secured to two leg braces that extend from the shaft. This device was designed to guide the limb through cyclic knee flexion-extension, while imposing (a) inertial or (b) elastic loads on the hamstrings. The inertial loads were imposed using high density inertial disks and induced an active lengthening contraction.

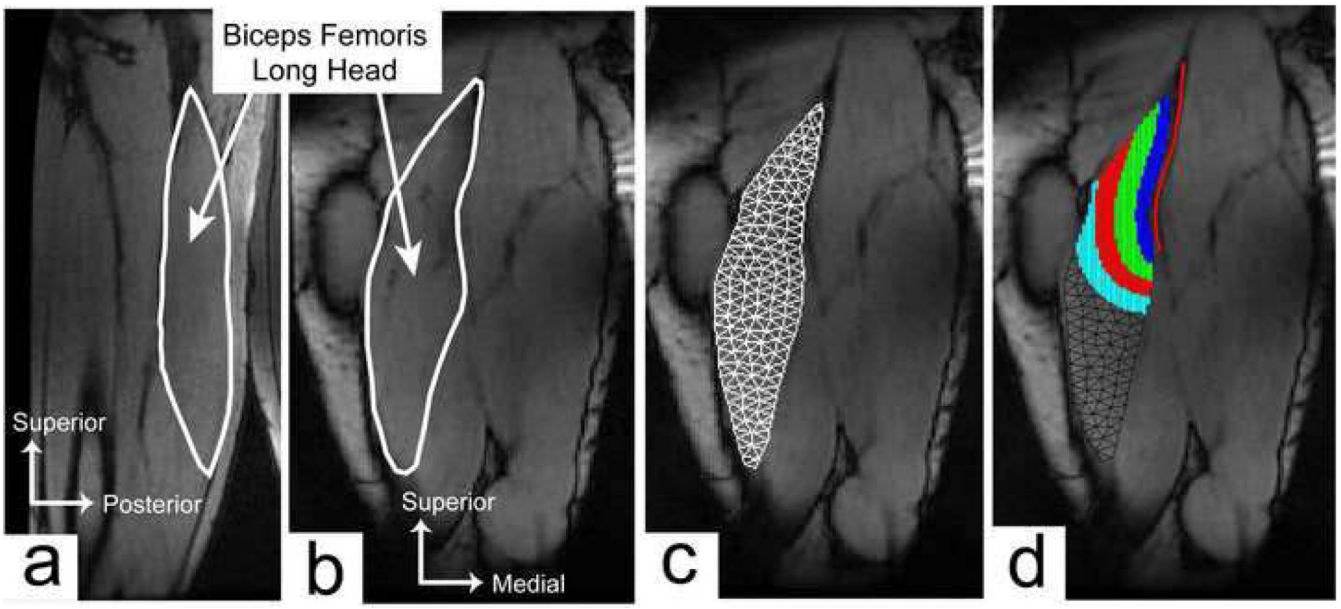

Figure 3.

Cine phase contrast imaging was used to measure muscle tissue velocities in either a (a) sagittal-oblique or (b) coronal-oblique imaging plane. (c) A mesh based tracking approach was used to compute tissue motion within the long head of the biceps femoris, relative to the muscle configuration in full knee flexion. (b) Four distinct spatial regions were defined for each subject (shaded regions), based on distance from the proximal tendon/aponeurosis (solid line). This allowed for quantitative analysis of displacement and strain measures relative to the musculotendon junction.

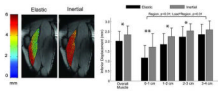

Figure 4.

(a) Maximum inferior displacements for the elastic and inertial loading conditions taken from a representative subject. More uniform displacement fields were observed when the hamstrings were subjected to an inertial load, compared to the elastic load. (b) Ensemble averaged data revealed relatively larger tissue motion for the inertial loading condition in the three regions nearest to the proximal musculotendon junction, when compared to the elastic loading condition. Overall tissue displacements across the entire muscle were significantly greater for the inertial loading, compared to the elastic loading. Abbreviations: * $p<0.05$; ** $p<0.01$

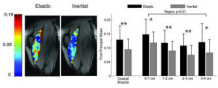

Figure 5.

(a) Shown is the computed first principal strain (E_1) field across the muscle at the time of peak knee extension under both elastic and inertial loading conditions for one representative subject. (b) For both loading conditions and across both subject groups, significantly larger strain magnitudes were observed in the tissue nearest to the proximal musculotendon junction. Overall muscle tissue strains were significantly smaller for the inertial loading condition, which reflects the muscle tissue remaining more isometric throughout the knee flexion-extension cycle. Abbreviations: *$p<0.05$; **$p<0.01$

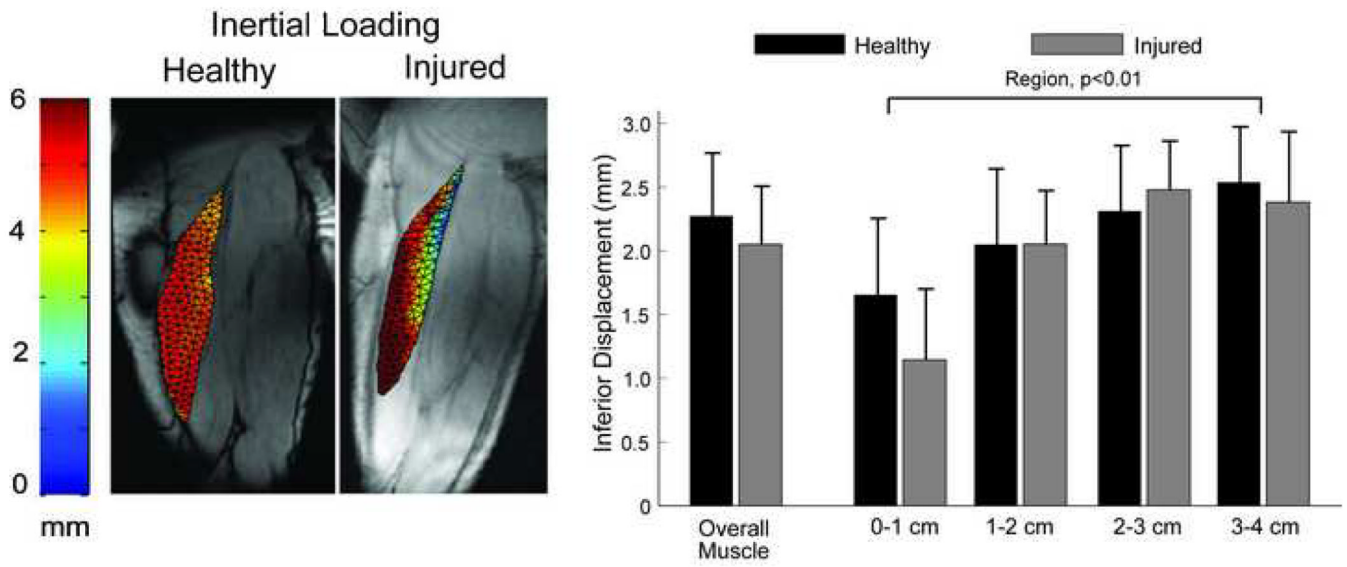

Figure 6.

(a) A sample image of the maximum inferior tissue displacements during the inertial loading for both a healthy and previously injured subject. The most notable difference is the smaller magnitude of motion along the proximal musculotendon junction. (b) Across all subjects, there was a significant spatial variation in motion across regions, with the previously injured subjects exhibiting less motion in the muscle tissue nearest the musculotendon junction.

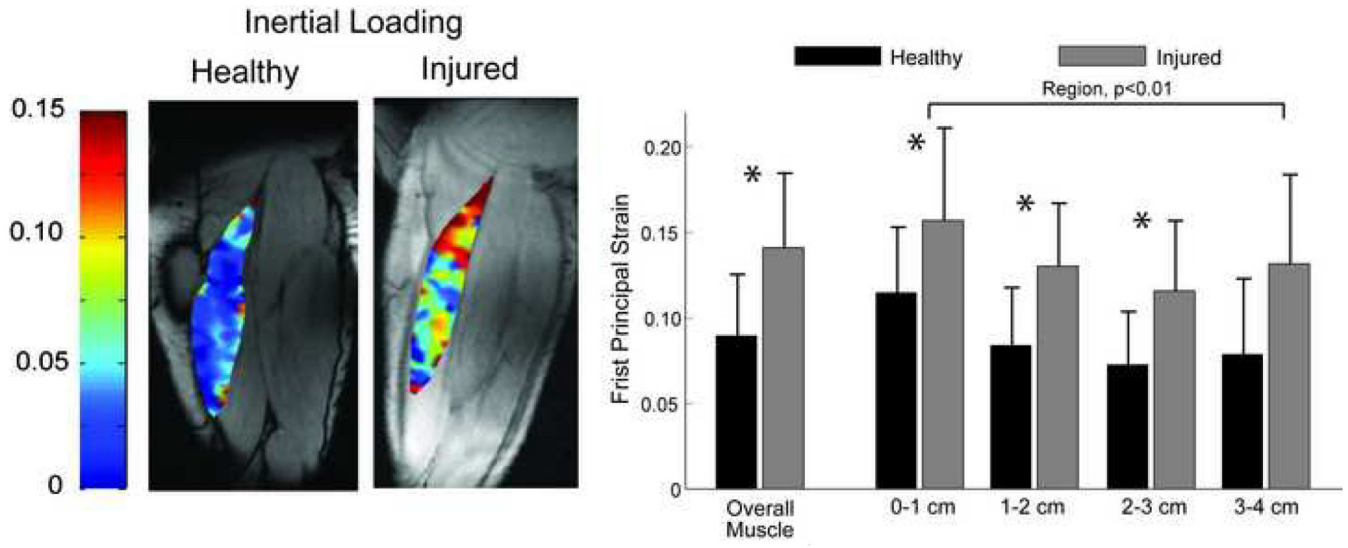

Figure 7.

(a) Representative images of the maximum first principal strains (E_1) in the biceps femoris for one healthy and one injured subject for the inertial loading condition. Larger strains were observed proximally in the previously injured subjects, compared to the un-injured subjects. (b) As a group, the previously injured subjects exhibited significantly larger first principal strains in the first three regions nearest the musculotendon junction, as well as the entire visible biceps femoris long head muscle tissue. Abbreviation: *$p<0.05$

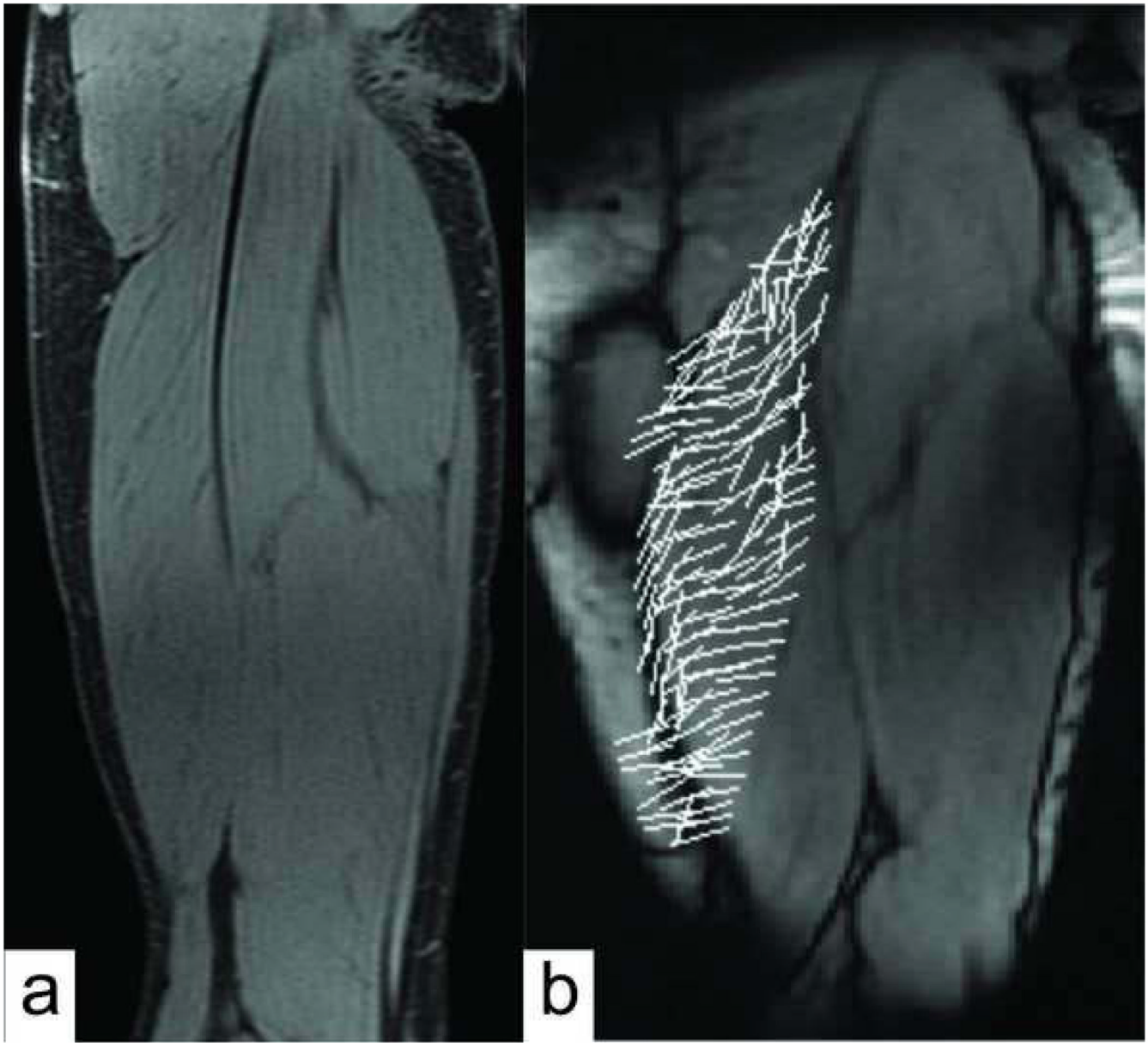

Figure 8.
(a) High resolution water-only static IDEAL images were obtained for all subjects and can be used to visualize muscle fascicle direction within the imaging plane. (b) The directions of the first principal strains seemed to generally align with fascicle direction within the main muscle body, suggestive that along fiber stretch was primarily occurring.